Disruption of TRPM6/TRPM7 complex formation by a mutation in the *TRPM6* gene causes hypomagnesemia with secondary hypocalcemia

Vladimir Chubanov*, Siegfried Waldegger†, Michael Mederos y Schnitzler*, Helga Vitzthum‡, Martin C. Sassen†, Hannsjörg W. Seyberth†, Martin Konrad†, and Thomas Gudermann*§

*Institute for Pharmacology and Toxicology, Philipps University Marburg, 35033 Marburg, Germany; †University Children's Hospital, Philipps University Marburg, 35037 Marburg, Germany; and ‡Department of Physiology I, University of Regensburg, 93040 Regensburg, Germany

Edited by Lily Y. Jan, University of California School of Medicine, San Francisco, CA, and approved December 18, 2003 (received for review August 15, 2003)

Impaired magnesium reabsorption in patients with *TRPM6* gene mutations stresses an important role of TRPM6 (melastatin-related TRP cation channel) in epithelial magnesium transport. While attempting to isolate full-length TRPM6, we found that the human *TRPM6* gene encodes multiple mRNA isoforms. Full-length TRPM6 variants failed to form functional channel complexes because they were retained intracellularly on heterologous expression in HEK 293 cells and *Xenopus* oocytes. However, TRPM6 specifically interacted with its closest homolog, the Mg^{2+}-permeable cation channel TRPM7, resulting in the assembly of functional TRPM6/TRPM7 complexes at the cell surface. The naturally occurring S141L TRPM6 missense mutation abrogated the oligomeric assembly of TRPM6, thus providing a cell biological explanation for the human disease. Together, our data suggest an important contribution of TRPM6/TRPM7 heterooligomerization for the biological role of TRPM6 in epithelial magnesium absorption.

Investigations on *Drosophila* flies with impaired vision due to mutations in the transient receptor potential gene (*trp*) initiated a search for homologous proteins in mammals, leading to the discovery of three subfamilies of cation channels: TRPCs (canonical or classical TRPs), TRPVs (vanilloid receptor and related proteins), and TRPMs (melastatin and related proteins) (1, 2). TRPC channels mediate cation entry in response to phospholipase C activation, whereas TRPV proteins respond to physical and chemical stimuli, such as temperature, pH, and mechanical stress (3, 4). Within their respective subfamilies, TRPCs and TRPVs form homo- and heterotetramers displaying novel pore properties when compared to their homomultimeric counterparts (1, 5–9). The eight TRPM family members differ significantly from the aforementioned TRP channels in terms of domain structure, cation selectivity, and activation mechanisms (3, 10). Two TRPM proteins, TRPM6 and TRPM7, harbor serine/threonine kinase domains in their C termini (11–16). Furthermore, TRPM7 displays unusual permeation properties by conducting a range of divalent metal ions including Mg^{2+} and Mn^{2+} (13, 17, 18).

It was recently shown that autosomal recessive hypomagnesemia with secondary hypocalcemia (HSH) is caused by mutations in the *TRPM6* gene (15, 16). HSH is characterized by low serum Mg^{2+} levels due to defective intestinal absorption or/and renal wasting of Mg^{2+}. Here we demonstrate that TRPM6 requires assembly with TRPM7 to form channel complexes in the cell membrane and that disruption of multimer formation by a mutated TRPM6 variant, TRPM6(S141L), results in human disease.

Methods

Molecular Biology and Generation of TRPM6 Polyclonal Antisera. The cloning procedure of human TRPM6 isoforms (Table 1) as well as amplification of other TRPM cDNAs is described in detail in *Supporting Methods*, which is published as supporting information on the PNAS web site. For TRPM proteins C-terminally fused to cyan (CFP) or yellow (YFP) fluorescent proteins, STOP codons in TRPMs were replaced by *Xho*I restriction sites through site-directed mutagenesis (QuikChange, Stratagene) followed by in-frame subcloning of CFP/YFP cDNAs. Fusion proteins containing CFP or YFP at the extreme N terminus of TRPM7 were constructed by exchanging the ATG start codon for a *Bam*HI restriction site. The procedure of RT-PCR-based analysis of microdissected rat nephron segments was performed as described (15). A polyclonal TRPM6-specific antiserum was produced in rabbits with the following peptide coupled to KLH: H_2N-ARETGRNSPEDDMQL-COOH (Standard immunization program, Eurogentec, Brussels).

Cell Culture, Assessment of Mn^{2+} Entry, Fluorescence Resonance Energy Transfer (FRET) Recordings, and Imaging of Subcellular Localization Patterns of TRPM6 and TRPM7. HEK 293 cells were cultured in Eagle's MEM supplemented with 10% FCS (PAA Laboratories, Pasching, Austria). For transient expression, HEK 293 cells grown on 25-mm glass coverslips in 35-mm dishes were cotransfected with an expression plasmid DNA mixture as indicated in the figure legends by using the METAFECTENE transfection reagent (Biontex Laboratories, Munich).

Measurements of Mn^{2+} entry in HEK 293 cells were performed 16–18 h after transfection. Cells were loaded with 5 μM fura-2 acetoxymethyl ester (Sigma) in Hepes-buffered saline (HBS; 140 mM NaCl/6 mM KCl/1 mM $MgCl_2$/2 mM $CaCl_2$/10 mM Hepes/5 mM glucose/0.1% BSA, pH 7.4) at room temperature for 45 min. After an additional 15-min incubation in HBS, cells were used for measurements within 1 h. Fura-2 fluorescence was recorded at room temperature at the isosbestic point (360 nm, 1-s intervals) with a Polychrome IV monochromator and an IMAGO II peltier-cooled charge-coupled device (CCD) camera (TILL Photonics, Planegg, Germany) coupled to an inverted IX70 microscope equipped with an UApo 340 40×/1.35 oil objective (Olympus, Melville, NY).

Our static FRET protocol was based on donor (CFP) fluorescence recovery after acceptor (YFP) bleach as reported (5). Cells were examined at room temperature in HBS with the setup used for fura-2 experiments except for a dual band-pass dichroic mirror and an emission-filter wheel (Lambda 10-2, Sutter Instruments, Novato, CA) included in the emission path to simul-

This paper was submitted directly (Track II) to the PNAS office.

Abbreviations: CFP, cyan fluorescent protein; FRET, fluorescence resonance energy transfer; HSH, hypomagnesemia with secondary hypocalcemia; YFP, yellow fluorescent protein.

Data deposition: The sequences reported in this paper have been deposited in the GenBank database [accession nos. AY333282 (TRPM6a), AY333283 (TRPM6b), AY333284 (TRPM6c), AY333285 (TRPM6a-t), AY333286 (M6-kinase 1), AY333287 (M6-kinase 2), AY333288 (M6-kinase 3), and NM_021450 (TRPM7)].

§To whom correspondence should be addressed at: Institute for Pharmacology and Toxicology, Philipps University Marburg, Karl-von-Frisch Strasse 1, 35033 Marburg, Germany. E-mail: guderman@staff.uni-marburg.de.

© 2004 by The National Academy of Sciences of the USA

Table 1. Cloned human TRPM6 isoforms

Name of isoform	Differences in splicing of transcripts	Length of ORF, aa	Accession no.
TRPM6a	Alternative first exon, 1A	2,022	AY333282
TRPM6b	Alternative first exon, 1B	2,017	AY333283
TRPM6c	Alternative first exon, 1C	2,017	AY333284
TRPM6t	Testis-specific variant containing an exon 36B harboring a STOP codon	1,943	AY333285
M6-kinase 1	In-frame splicing of exon 14 to exon 28	973	AY333286
M6-kinase 2	In-frame splicing of exon 13 to exon 30	855	AY333287
M6-kinase 3	In-frame splicing of exon 7 to exon 34	569	AY333288

taneously record YFP and CFP fluorescence. Student's *t* test was used for statistical analysis.

Living cells, transiently expressing YFP-tagged proteins, were directly examined by confocal microscopy 24 h after transfection. Confocal images were obtained with a TCS SP2 laser scanning microscope (Leica, Deerfield, IL). We used a 63×/1.32 oil objective (PL Apo Ph3 CS), the 488-nm excitation wavelength of an argon laser, and a dichroic filter allowing for a detection bandwidth of 500–600 nm.

Expression of TRPM Proteins in *Xenopus laevis* Oocytes. TRPM cDNAs were subcloned into the pOGII vector (a pBluescript derivative with the 5′ and 3′ UTRs of *Xenopus* β-globin). Ten nanograms of *in vitro* transcribed cRNA (mMESSAGE mMACHINE kit, Ambion, Austin, TX) for each TRPM construct was injected into defolliculated *Xenopus* oocytes, which were kept in ND96 solution containing 96 mM NaCl, 2 mM KCl, 1.8 mM $CaCl_2$, 1 mM $MgCl_2$, 5 mM Hepes (pH 7.4), 2.5 mM sodium pyruvate, 0.5 mM theophylline, and 20 μg/ml gentamicin at 16°C. Two to five days after injection, two-electrode voltage-clamp measurements were performed with a GeneClamp 500 amplifier (Axon Instruments, Foster City, CA) at room temperature. Currents were recorded in ND96 solution without sodium pyruvate, theophylline, and gentamicin. Data shown in the paper were reproduced in at least two different batches of oocytes. Statistical analysis was performed on oocytes derived from one preparation with at least seven oocytes per data point by using Student's *t* test.

For determination of TRPM6 surface expression, a highly purified plasma membrane fraction was prepared as described (19). Western blot analysis of membrane protein extracts for the presence of TRPM6 was performed with the above described TRPM6 polyclonal antiserum.

Results

Identification of Multiple TRPM6 Isoforms Displaying Overlapping Expression Patterns with TRPM7. While seeking to isolate full-length human TRPM6 cDNAs, we obtained a variety of alternative gene products (Fig. 1*A* and Table 1). Surprisingly, 5′ rapid amplification of cDNA ends (5′ RACE) revealed three short alternative 5′ exons, called 1A, 1B, and 1C, that were found to be individually spliced onto exon 2 (Fig. 1*A*). All three 5′ exons are located within a 700-bp region on chromosome 9q22 (Fig. 6, which is published as supporting information on the PNAS web site), suggesting that the *TRPM6* gene harbors a promoter with alternative transcription start sites. The newly identified 5′ exons prompted us to denominate the full-length isoforms *TRPM6a*, *TRPM6b*, and *TRPM6c* (Table 1). *TRPM6a/b/c* variants are spliced from 39 exons coding for >2,000 aa (Fig. 1 and Table 1). Apart from the large conserved N-terminal domain, full-length

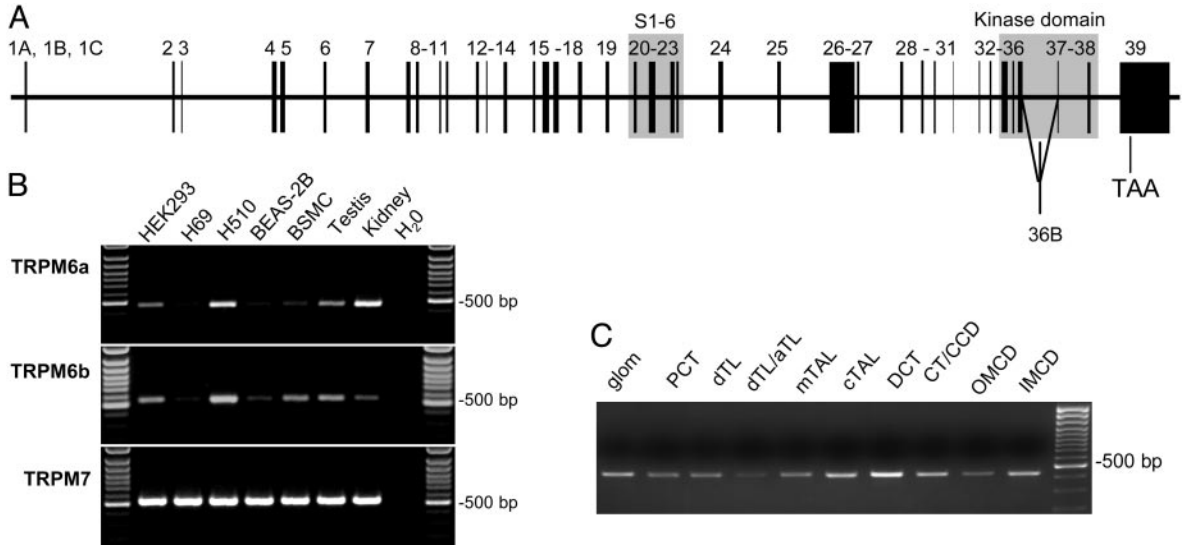

Fig. 1. Human TRPM6 gene structure and expression pattern of TRPM6 and TRPM7. (*A*) Intron–exon structure of the human TRPM6 gene according to the primary sequence analysis of cDNA variants cloned. Exons encoding putative transmembrane domains (S1–6) and the predicted kinase domain are highlighted by a gray background. Exon 36B, spliced between exon 36 and 37, was detected only in mRNA from human testis. (*B*) Diagnostic RT-PCR for TRPM6a, TRPM6b, and TRPM7 mRNA expression in HEK 293, H69, and H510 small cell lung carcinoma cells as well as in human bronchial epithelial cells (BEAS-2B), human bronchial smooth muscle cells (BSMC), human testis, and human kidney. (*C*) Diagnostic TRPM7 RT-PCR on microdissected rat nephron segments, including glomeruli (glom), proximal convoluted tubule (PCT), descending thin limb (dTL), ascending TL (aTL), medullary thick ascending limb (mTAL), cortical TAL (cTAL), distal convoluted tubule DCT, connecting tubule/cortical collecting duct (CT/CCD), outer medullary collecting duct (OMCD), and inner medullary collecting duct (IMCD).

TRPM6 isoforms each harbor a hexahelical TRP-like channel segment and an α-kinase domain (20) in the C terminus. Full-length TRPM6 variants are closely related to TRPM7 with >50% of overall sequence identity (Fig. 7*C*, which is published as supporting information on the PNAS web site). Also, we isolated three alternatively spliced isoforms lacking internal exons encoding the hexahelical transmembrane domain (Table 1 and Fig. 7). We called these isoforms M6-kinases 1, 2, and 3 to account for their homology to *m*elastatin within the conserved N-terminal regions on the one hand and for the presence of a C-terminal *kinase* domain on the other.

To shed further light on the cellular role of TRPM6 variants, we examined their expression pattern by RT-PCR. Sense primers were located in the alternative first exons, ensuring that PCR products were amplified only from specific TRPM6 isoforms (*Supporting Methods*). We noted that two isoforms, *TRPM6a* and *TRPM6b*, were coexpressed with TRPM7 in human kidney, testis, and HEK 293 cells, and in several cell lines of lung origin (Fig. 1*B*). Interestingly, the *TRPM6c* variant was detected only in H510 small cell lung carcinoma cells and human testis (Fig. 7*B*). TRPM6 has been invoked as an essential molecular component of active transcellular Mg^{2+} absorption in the gut and kidney, and TRPM6 mRNA is expressed in discrete locations along the rat nephron, i.e., proximal convoluted tubule, distal convoluted tubule, and collecting duct (15). To see whether TRPM6 and TRPM7 were also coexpressed in the kidney nephron, we subjected total mRNA isolated from microdissected rat nephrons to RT-PCR analysis and detected TRPM7 mRNA in all nephron segments tested (Fig. 1*C*). Our findings concur with previous reports on a widespread expression pattern of TRPM7 with highest levels in kidney (13) and detection of TRPM6 transcripts by Northern blot in lung, kidney, and testis (16). Thus, in all cells and tissues tested so far, TRPM6 expression invariably occurs on the background of a ubiquitous presence of TRPM7.

Heterologous Expression of TRPM6 and TRPM7 in *Xenopus* Oocytes. For functional analysis, we injected cRNAs derived from full-length TRPM6 variants as well as from TRPM7 into *Xenopus* oocytes and compared the electrophysiological properties of TRPM6-expressing oocytes to those injected with TRPM7 cRNA under two-electrode voltage-clamp conditions (Fig. 2). Expression of TRPM7 resulted in the development of inward and outward currents at negative and positive voltages, respectively. Outward cation currents exhibited pronounced rectification at positive potentials (Fig. 2*A*) reminiscent of the behavior of TRPM7 when expressed in mammalian cell lines (11, 13). As opposed to TRPM7, TRPM6a cRNA injection did not entail significant ion currents compared to water-injected control oocytes (Fig. 2*A*). Similar results were obtained for the TRPM6b and TRPM6c variants (data not shown). Because of their overlapping expression pattern, we reasoned that TRPM6 and TRPM7 might assemble into heteromultimeric complexes, which would impinge on functional channel characteristics. In fact, coexpression of TRPM6 and TRPM7 resulted in an amplification of the TRPM7-like currents, most pronounced at positive membrane voltages (Fig. 2*A*).

Whereas most HSH mutations of the TRPM6 gene either are nonsense or frameshift mutations easily compatible with a loss-of-function phenotype, one missense mutation entails the exchange of a highly conserved serine for a leucine residue at amino acid position 141 (15). To disclose the molecular mechanism underlying the genetically proven functional deficit of TRPM6(S141L), we coinjected TRPM7 and TRPM6(S141L) cRNA and noted that the current amplification mediated by TRPM6/TRPM7 coexpression in *Xenopus* oocytes was lost when wild-type TRPM6 was replaced by the naturally occurring mutant (current amplitudes at +40 mV: TRPM7, 1028 ± 143 nA; TRPM6/TRPM7, 1446 ± 84 nA; TRPM6(S141L)/TRPM7, 909 ± 71 nA; $n = 14$).

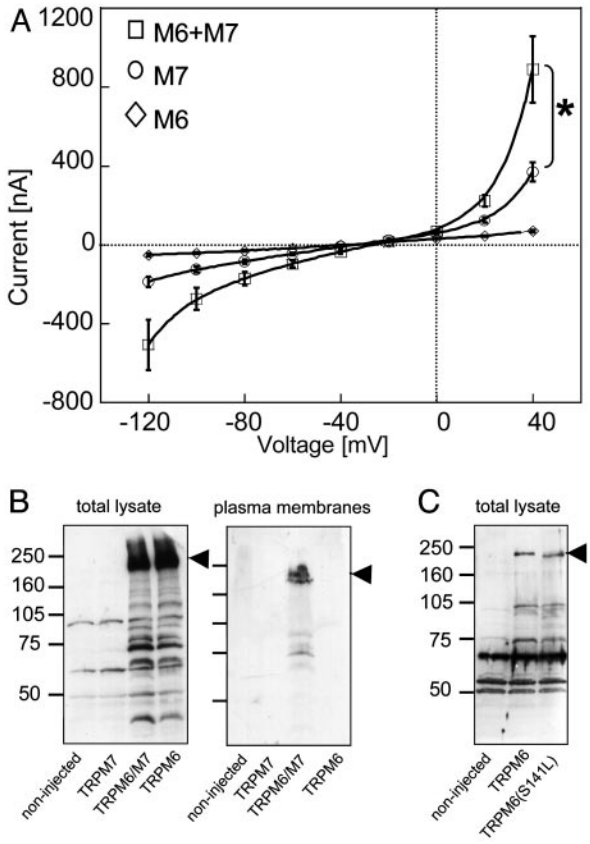

Fig. 2. Heterologous expression of TRPM6/7 in *Xenopus* oocytes. (*A*) Two-electrode voltage clamp analysis of oocytes injected with 10 ng of cRNA encoding TRPM6 (M6), TRPM7 (M7), or 10 ng of TRPM6 together with 10 ng of TRPM7 cRNA (M6+M7). *I–V* relationships were determined on at least seven oocytes per *I–V* curve. *, $P < 0.05$. (*B*) Western blot analysis of TRPM6 expression in total lysates (*Left*) and in plasma membranes (*Right*) of *Xenopus* oocytes, using a TRPM6-specific antiserum. (*C*) Western blot analysis of TRPM6 and TRPM6(S141L) expression in total lysates of *Xenopus* oocytes. The positions of TRPM6-specific bands are indicated by arrowheads.

To acquire independent evidence in support of our functional data, we coinjected TRPM6a and TRPM7 cRNAs in oocytes and assessed the level of TRPM6a protein in total lysates and in the plasma membrane fraction by Western blot (Fig. 2*B*). In accord with the obtained electrophysiological recordings, TRPM6a was present in the cell lysate but absent from the plasma membrane, whereas coinjection of TRPM6a and TRPM7 cRNA allowed for the detection of TRPM6 protein in the cell membrane fraction (Fig. 2*B*). Also, we found that the expression level of TRPM6a protein was affected neither by coexpression of TRPM7 nor by the missense S141L mutation (Fig. 2*C*), ruling out the possibility that the observed biophysical differences were influenced by the expression level of TRPM proteins.

These findings indicate that TRPM6 subunits are unable to form a functional channel complex in the *Xenopus* cell membrane when expressed alone, whereas TRPM7 is able to usher TRPM6 to the cell membrane, presumably by forming mixed multimers.

Cotrafficking of TRPM6 and TRPM7 to the Cell Surface in HEK 293 Cells. To exclude that the cellular trafficking deficit of TRPM6 was a unique property of *Xenopus* oocytes, we extended our investigations to mammalian cells. TRPMs were C-terminally fused

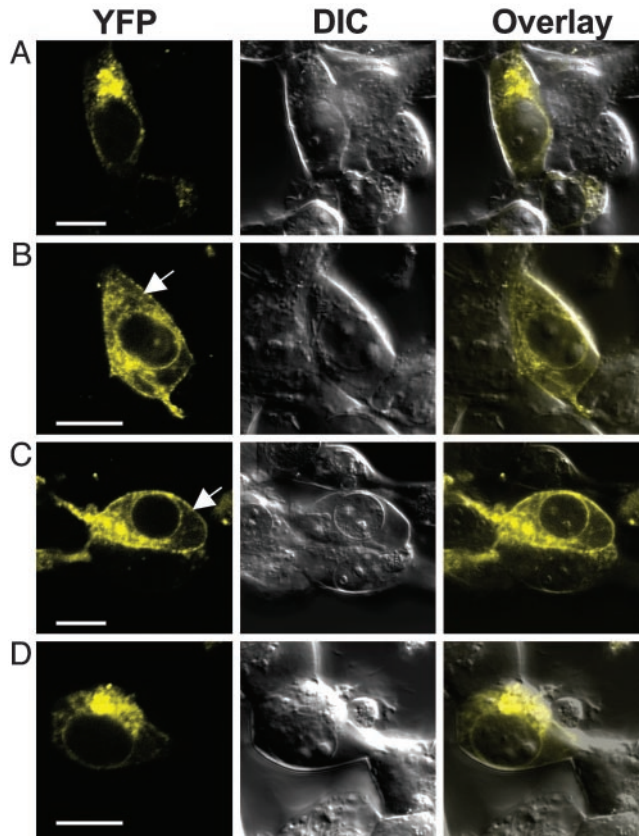

Fig. 3. Subcellular localization of transiently expressed TRPM6 and TRPM7 in living HEK 293 cells. TRPM6 and TRPM7 were C-terminally fused to YFP and transiently expressed in HEK 293 cells. TRPM6-YFP (*A*) and TRPM7-YFP (*B*) were expressed alone; TRPM6-YFP (*C*) and TRPM6(S141L)-YFP (*D*) were coexpressed with untagged TRPM7 at a ratio of 1:3 (YFP-tagged/untagged cDNAs). Images of YFP fluorescence (YFP), the corresponding differential interference contrast images (DIC), and overlays of both are depicted. (Scale bars, 10 μm.) The arrow indicates the plasma membrane. Typical examples of three independent transfections are shown.

in-frame to YFP and resulting constructs were transiently expressed in HEK 293 cells (Fig. 3). Confocal laser scanning microscopy of living cells revealed TRPM6a-YFP to be exclusively localized within intracellular membrane compartments of examined cells (Fig. 3*A*). On the contrary, 39 ± 4% (n = 4) of TRPM7-YFP-transfected cells showed a discrete plasma membrane staining (Fig. 3*B*). Of note, when TRPM6a-YFP was coexpressed with untagged TRPM7, fluorescence labeling of the plasma membrane was discernible in 43 ± 13% (n = 4) of transfected cells, indicative of a TRPM7-mediated insertion of TRPM6a-YFP into the cell membrane (Fig. 3*C*). TRPM7-dependent cellular trafficking of TRPM6a proved to be specific, because no other TRPM protein tested (human TRPM1, TRPM2, and TRPM4B, and mouse TRPM5) was sufficient to promote cell membrane insertion of TRPM6a-YFP on coexpression (data not shown). In line with our functional data acquired in *Xenopus* oocytes, the intracellular distribution pattern of TRPM6a(S141L)-YFP coexpressed with TRPM7 remained unaffected (Fig. 3*D*), suggesting that the S141L mutation prevented the assembly of TRPM6a/TRPM7 heteromultimers, a process that appears to be required for cell membrane targeting of TRPM6a. Next, we resorted to fluorescence-activated cell sorting analysis of HEK 293 cells transiently expressing YFP-labeled proteins to investigate the expression level of recombinant TRPM proteins. In line with data obtained in *Xenopus* oocytes (Fig. 2*B*), we did not observe differences in the expression level of TRPM6a(S141L)-YFP, TRPM6a-YFP, and TRPM7-YFP (Fig. 8, which is published as supporting information on the PNAS web site). Using this approach, we also found that TRPM6 did not increase TRPM7-YFP expression. To exclude the possibility that the intracellular retention of TRPM6a was caused by the YFP tag, we performed immunofluorescent staining of transiently transfected HEK 293 cells by using either TRPM6- or TRPM7-specific antisera, thereby confirming our observations with fluorophore-tagged fusion proteins (Fig. 9, which is published as supporting information on the PNAS web site). Finally, to prove that the S141L missense mutation in TRPM6 is indeed responsible for the trafficking incompetence of the protein, we performed a homologous S138 to L exchange in TRPM7. Mutation of this amino acid, which is highly conserved within the TRPM subfamily, resulted in the retention of TRPM7(S138L) in intracellular membrane compartments (Fig. 9).

Thus, TRPM6 specifically requires TRPM7 for trafficking to the cell surface, most probably by means of mixed heteromer formation. Moreover, impaired cotargeting of TRPM6(S141L) by TRPM7 suggests that the molecular basis of the HSH phenotype involves a trafficking or/and multimerization deficit of TRPM6(S141L).

Heteromultimerization of TRPM6 and TRPM7 as Assessed by Mn^{2+} Entry and FRET. TRPM7 has been characterized as a constitutively active nonselective cation channel permeable for divalent metal trace ions including Mn^{2+} (18). To functionally assess the proposed formation of TRPM6/TRPM7 heteromers, we added 1 mM Mn^{2+} to the bath solution and recorded the influx of Mn^{2+} ions into transfected HEK 293 cells by means of fura-2 fluorescence quenching (Fig. 4*A*). As depicted in Fig. 4*A*, the basal rate of Mn^{2+} entry did not differ between control and TRPM6a-expressing cells (Fig. 4 *A* and *B*). However, expression of TRPM7 caused substantial quenching of the fura-2 signal. Most notably, the rate of Mn^{2+} entry was further increased by coexpression of TRPM6a and TRPM7, whereas TRPM6(S141L) did not enhance TRPM7-mediated Mn^{2+} entry (Fig. 4*B*).

To demonstrate direct protein–protein interactions between TRPM proteins, we took advantage of a FRET-based approach, which has recently been shown to reliably describe TRP subunit assembly (5, 6). We used C-terminal fusion constructs of TRPMs with CFP or YFP and assessed the proximity of coexpressed TRP proteins differentially tagged on their C termini by FRET. The FRET signal was recorded quantitatively under static conditions by monitoring the increase in donor (CFP) emission during selective photobleach of the acceptor fluorophore (YFP) (Fig. 5).

We observed a homomultimeric interaction of TRPM6 as well as TRPM7 (Fig. 5 *A* and *C*). Also, we detected FRET between coexpressed TRPM6a-CFP and TRPM7-YFP. Introduction of the S141L missense mutation into TRPM6 abrogated homo- and heterooligomeric complex formation (Fig. 5*C*). The TRPM6/TRPM7 interaction was specific because we failed to record FRET when TRPM6a was coexpressed with other members of the TRP family, i.e., TRPC6 and TRPM1 (Fig. 5*B*). Thus, we conclude that TRPM6a directly interacts with TRPM7 to form a functional channel complex on the cell surface, whereas TRPM6(S141L) interferes with the formation of an oligomeric protein complex and, therefore, is retained intracellularly.

Discussion

The subfamily of melastatin-related TRP cation channels (TRPM) consists of eight gene products characterized by distinct ion permeation properties and different modes of regulation. TRPM7 appears to fulfill a central, ubiquitous role to mediate Mg^{2+} uptake in vertebrate cells (17). Additionally, it has recently

CELL BIOLOGY

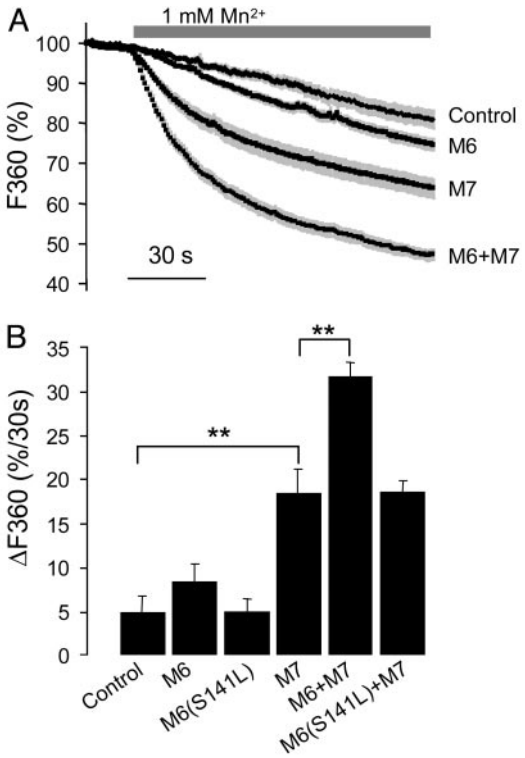

Fig. 4. TRPM6- and TRPM7-mediated Mn^{2+} entry in HEK 293 cells. HEK 293 cells were transiently cotransfected with plasmids (50 ng) encoding GFP and a mixture of plasmid DNAs as indicated: Control, 2 μg of empty pcDNA3.1 vector; M6, 1 μg of TRPM6 plus 1 μg of pcDNA3.1; M7, 1 μg of TRPM7 plus 1 μg of pcDNA3.1; M6+M7, 1 μg of TRPM6 plus 1 μg of TRPM7; M6(S141L)+M7, 1 μg of TRPM6(S141L) plus 1 μg of TRPM7. Bold black lines indicate calculated mean values of individual traces recorded from single cells, and gray lines depict the SEM obtained for each time point. Addition of 1 mM Mn^{2+} in HBS is indicated by a gray bar. Typical examples from four independent transfections are shown. (*B*) Rate of Mn^{2+} entry (percentage decrease of fluorescence at 360 nm over 30 sec) is presented as means and SEM calculated from four independent transfections. **, $P < 0.01$.

been demonstrated that TRPM6 is involved in epithelial Mg^{2+} transport, because patients suffering from HSH display mutations in the TRPM6 gene (15, 16). The effect of such mutations for TRPM6 function at the cellular level, however, has not been worked out.

In the course of the present study, we obtained several previously uncharacterized isoforms of human TRPM6, allowing us to unequivocally define the exon–intron structure of the TRPM6 gene. The close proximity of the three cloned 5′ exons within a 700-bp genomic region suggests that the TRPM6 gene is governed by a single core promoter using alternative transcription start sites, a phenomenon which has been implicated as a mechanism responsible for a tight regulation of gene function in the case of other ion channel promoters (21, 22). Alternative splicing of internal exons appears to be an intrinsic property of the TRPM gene subfamily. It should be noted, however, that the TRPM6 like the TRPM7 gene (11, 12) gives rise to two distinct types of proteins: (*i*) ion channels fused to a C-terminal kinase domain, and (*ii*) so-called M-kinases lacking the hexahelical transmembrane span. At present, a possible contribution of the kinase activity to ion channel function is a highly contentious issue (11, 13, 17). The expression of M6-kinases raises the possibility that the biological role of this atypical α-kinase domain may not necessarily be confined to modulation of the ion channel moiety. The reported interaction of the TRPM7 kinase

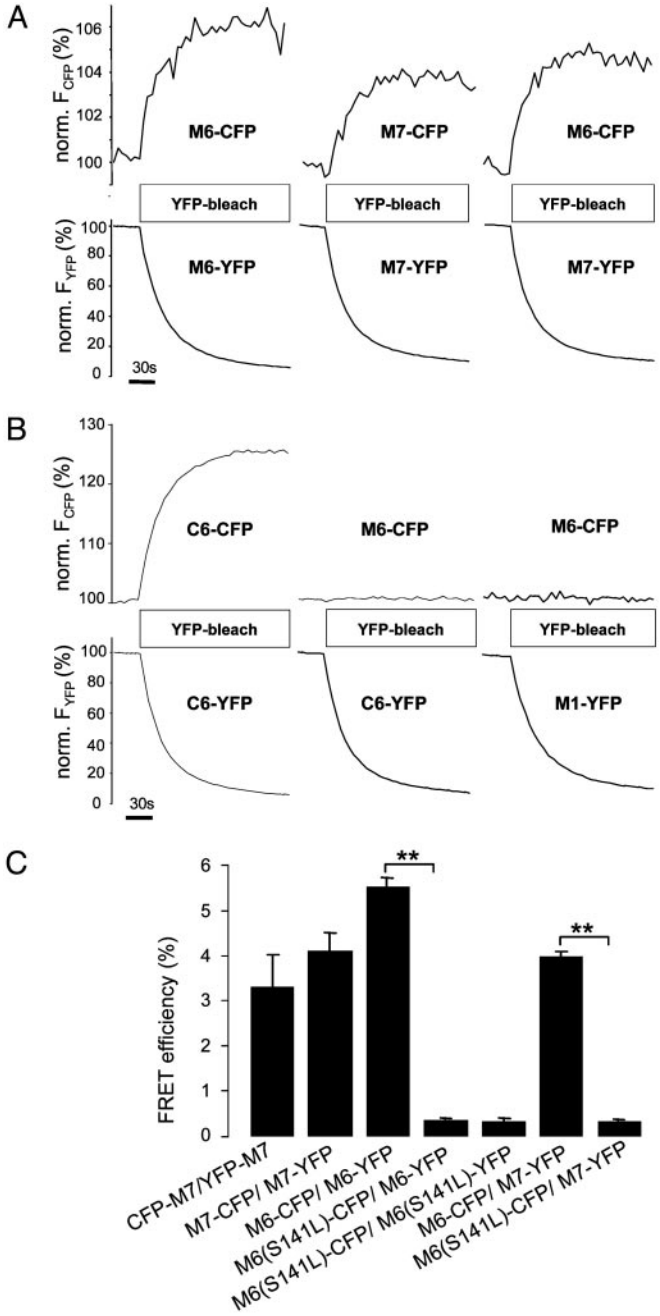

Fig. 5. TRPM6/7 assembly as assessed by FRET. (*A*) TRPM6 and TRPM7 C-terminally fused to CFP or YFP were coexpressed in HEK 293 cells. Static FRET signals were recorded between TRPM6-CFP/YFP (*Left*), TRPM7-CFP/YFP (*Center*), and TRPM6-CFP/TRPM7-YFP (*Right*). (*B*) Static FRET between TRPC6-YFP/TRPC6-CFP subunits was used as a positive control (*Left*). Other tested FRET combinations were TRPM6-CFP/TRPC6-YFP (*Center*) and TRPM6-CFP/TRPM1-YFP (*Right*). (*C*) Mean values and SEM of FRET efficiency were calculated from four independent transfections. **, $P < 0.01$.

domain with several phospholipase C isoforms lends further credence to such a possibility (11, 12).

It has recently been demonstrated that TRPM7 can conduct a broad array of divalent cations with conspicuous preference for Zn^{2+} and Ni^{2+} (18). The rather unusual permeability sequence includes Mg^{2+} as well (13, 18). In light of the disturbed Mg^{2+} homeostasis of HSH patients (15, 16) and the results presented in this study, we hypothesize that the two homologous TRPMs,

TRPM6 and TRPM7, may be functionally linked and both be involved in the process of epithelial Mg^{2+} absorption. Such an assumption is compatible with the overlapping expression pattern of TRPM6 and the ubiquitously expressed TRPM7 as deduced from Northern blot (13, 16) and RT-PCR analyses. Thus, in the kidney, where both TRPM6 and TRPM7 are prominently expressed, RT-PCR analysis on microdissected rat nephron segments detected TRPM6 mRNA in the proximal and distal convoluted tubules as well as in the collecting ducts (15), whereas we found TRPM7 transcripts in all nephron segments examined.

The overlapping expression pattern of TRPM6 and TRPM7 and their proposed involvement in cellular Mg^{2+} absorption prompted us to test whether the two TRPM proteins might be components of heterooligomeric ion channel complexes in the plasma membrane. The formation of mixed oligomers has already been demonstrated for members of the TRPC and TRPV subfamilies (5–9). Here, we present several independent lines of evidence to the effect that TRPM6 specifically interacts with TRPM7 to form a functional ion channel complex in the cell membrane. First, we found that all full-length TRPM6 isoforms, i.e., TRPM6a, -b, and -c, were retained intracellularly when expressed in *Xenopus* oocytes alone, but were incorporated into functionally active channel complexes in the plasma membrane on coexpression with TRPM7. Second, the marked enhancement of Mn^{2+} entry in HEK 293 cells expressing both TRPM6 and TRPM7 fully endorsed equivalent electrophysiological recordings in *Xenopus* oocytes. Third, detailed analysis of living and fixed HEK 293 cells highlighted the fact that TRPM6 requires the presence of TRPM7 to be targeted to the cell membrane. Fourth, direct protein–protein association of TRPM6 and TRPM7 was confirmed by a static FRET strategy. We have previously shown that TRPC subunits combine within the narrow confines of given subfamilies, i.e., exclusively within the TRPC1/4/5 and the TRPC3/6/7 group of channels (5). According to primary sequence similarity, the eight TRPM proteins fall into four distinct groups: TRPM6/7, TRPM1/3, TRPM4/5, and TRPM2/8 (Fig. 7). It is tempting to speculate that heteromeric channel complexes can only be formed within but not beyond these groups. While this paper was being revised, Voets *et al.* (23) reported a 4- to 7-fold amplification of TRPM7-like currents on overexpression of a human TRPM6 variant in HEK 293 cells. Assuming identical biophysical properties of TRPM6 and TRPM7, these ion currents might alternatively be interpreted to originate from TRPM6 homotetramers, although direct evidence is still lacking.

Another major finding of the present work relates to the analysis of TRPM6(S141L), the only missense loss-of-function mutation detected in HSH patients so far (15). In contrast to wild-type TRPM6a, the mutated protein failed to amplify TRPM7-mediated currents in *Xenopus* oocytes as well as Mn^{2+} entry in HEK 293 cells. Furthermore, TRPM6a(S141L) was not cotargeted to the cell surface by TRPM7 and did not yield a FRET signal with the coexpressed TRPM7. Therefore, we provide a molecular explanation for the genetically defined loss-of-function phenotype imparted by the S141L missense mutation in that the exchange of an amino acid residue in the proteins conserved N terminus abolishes complex formation with TRPM7 resulting in intracellular retention of TRPM6(S141L). How can the oligomerization/trafficking competence of TRPM6 be affected by mutation of S141, which is located far away from the putative transmembrane segment? It is tempting to speculate that the TRPM N terminus serves a similar role for the multimerization of ion channel subunits as the N-terminal T1 domains in voltage-gated K^+ channels (24).

Mg^{2+} is the second most abundant cation within eukaryotic cells and plays an essential physiological role as cofactor of numerous enzymes and modulator of ion channels and membrane transporters (25, 26). Intriguingly, little is known about the molecular components involved in transepithelial Mg^{2+} transport. However, the reported permeation properties and cellular role of TRPM7 (16, 19), the phenotype of HSH patients caused by TRPM6 mutations, and the functional link between these two TRPM proteins as highlighted in our study place strong emphasis on TRPM6/7 channel complexes as essential components of the epithelial Mg^{2+} uptake machinery whose detailed functional characteristics and regulation should be rewarding topics of future investigations. Disruption of multimeric ion channel complexes by a mutated TRPM6 variant, TRPM6(S141L), diagnosed in HSH patients, illuminates a facet of the cell biological basis of human disease.

We thank Berit Schuhmann for assistance in fluorescence-activated cell sorting analysis and Ludmila Sytik for technical assistance. This study was supported by the Deutsche Forschungsgemeinschaft and Fonds der Chemischen Industrie.

1. Hardie, R. C. (2001) *J. Exp. Biol.* **204,** 3403–3409.
2. Clapham, D. E., Montell, C., Schultz, G. & Julius, D. (2003) *Pharmacol. Rev.* **55,** 591–596.
3. Clapham, D. E. (2003) *Nature* **426,** 517–524.
4. Voets, T. & Nilius, B. (2003) *J. Membr. Biol.* **192,** 1–8.
5. Hofmann, T., Schaefer, M., Schultz, G. & Gudermann, T. (2002) *Proc. Natl. Acad. Sci. USA* **99,** 7461–7466.
6. Schaefer, M., Plant, T. D., Stresow, N., Albrecht, N. & Schultz, G. (2002) *J. Biol. Chem.* **277,** 3752–3759.
7. Goel, M., Sinkins, W. G. & Schilling, W. P. (2002) *J. Biol. Chem.* **277,** 48303–48310.
8. Hoenderop, J. G., Voets, T., Hoefs, S., Weidema, F., Prenen, J., Nilius, B. & Bindels, R. J. (2003) *EMBO J.* **22,** 776–785.
9. Strubing, C., Krapivinsky, G., Krapivinsky, L. & Clapham, D. E. (2001) *Neuron* **29,** 645–655.
10. Hofmann, T., Chubanov, V., Gudermann, T. & Montell, C. (2003) *Curr. Biol.* **13,** 1153–1158.
11. Runnels, L. W., Yue, L. & Clapham, D. E. (2001) *Science* **291,** 1043–1047.
12. Runnels, L. W., Yue, L. & Clapham, D. E. (2002) *Nat. Cell Biol.* **4,** 329–336.
13. Nadler, M. J., Hermosura, M. C., Inabe, K., Perraud, A. L., Zhu, Q., Stokes, A. J., Kurosaki, T., Kinet, J. P., Penner, R., Scharenberg, A. M. & Fleig, A. (2001) *Nature* **411,** 590–595.
14. Riazanova, L. V., Pavur, K. S., Petrov, A. N., Dorovkov, M. V. & Riazanov, A. G. (2001) *Mol. Biol. (Mosk.)* **35,** 321–332.
15. Schlingmann, K. P., Weber, S., Peters, M., Niemann Nejsum, L., Vitzthum, H., Klingel, K., Kratz, M., Haddad, E., Ristoff, E., Dinour, D., *et al.* (2002) *Nat. Genet.* **31,** 166–170.
16. Walder, R. Y., Landau, D., Meyer, P., Shalev, H., Tsolia, M., Borochowitz, Z., Boettger, M. B., Beck, G. E., Englehardt, R. K., Carmi, R. & Sheffield, V. C. (2002) *Nat. Genet.* **31,** 171–174.
17. Schmitz, C., Perraud, A. L., Johnson, C. O., Inabe, K., Smith, M. K., Penner, R., Kurosaki, T., Fleig, A. & Scharenberg, A. M. (2003) *Cell* **114,** 191–200.
18. Monteilh-Zoller, M. K., Hermosura, M. C., Nadler, M. J., Scharenberg, A. M., Penner, R. & Fleig, A. (2003) *J. Gen. Physiol.* **121,** 49–60.
19. Kamsteeg, E. J. & Deen, P. M. (2001) *Biochem. Biophys. Res. Commun.* **282,** 683–690.
20. Ryazanov, A. G., Pavur, K. S. & Dorovkov, M. V. (1999) *Curr. Biol.* **9,** R43–R45.
21. Wickman, K., Pu, W. T. & Clapham, D. E. (2002) *Gene* **284,** 241–250.
22. Mouchel, N., Broackes-Carter, F. & Harris, A. (2003) *Hum. Mol. Genet.* **12,** 759–769.
23. Voets, T., Nilius, B., Hoefs, S., van der Kamp, A. W., Droogmas, G., Bindels, R. J. & Hoenderop, J. G. (2004) *J. Biol. Chem.* **279,** 19–25.
24. Minor, D. L., Lin, Y. F., Mobley, B. C., Avelar, A., Jan, Y. N., Jan, L. Y. & Berger, J. M. (2000) *Cell* **102,** 657–670.
25. Quamme, G. A. & de Rouffignac, C. (2000) *Front. Biosci.* **5,** D694–D711.
26. Dai, L. J., Ritchie, G., Kerstan, D., Kang, H. S., Cole, D. E. & Quamme, G. A. (2001) *Physiol. Rev.* **81,** 51–84.